Fourier Neural Operator for Parametric Partial Differential Equation in Tumor Growth Prediction

Walia Farzana

***Abstract*— Partial differential equation (PDE) of reaction-diffusion type is applied to model the tumor growth, which describes the spatial distribution of tumor cell density and tumor behavior: proliferation and infiltration. Traditional PDE solver such as finite element methods (FEM) and finite difference methods (FDM) rely on discretizing the space into a very fine mesh which can be slow and inefficient. The neural operator is mesh-independent, different from the standard deep learning methods such as Convolutional Neural Network (CNN). It can be trained on one mesh and evaluated on another. By parameterizing the model in function space, it learns the continuous function instead of discretized vectors. Fourier neural operator (FNO) leverages neural networks with Fourier transforms to map its input function to the target function in the frequency domain, showcasing notably superior performance compared to traditional CNNs. The design of FNO utilizes global Fourier filters, whereas CNNs rely on local filters. Formulating a neural operator by parameterizing the integral kernel directly in Fourier space, allows an efficient architecture. We propose to perform experiments on reaction-diffusion PDE for tumor growth model. The proposed framework will apply FNO on the initial tumor density map to predict final tumor growth. The model performance will be evaluated using different model evaluation metrics and optimization functions. The results with simulated data exhibits that CNN performs better with image-specific loss function.**

Keywords- Fourier Neural Operator, Tumor Growth, Partial Differential Equation(PDE).

I. INTRODUCTION

Partial differential equations (PDEs) serve as the fundamental mathematics tools for modeling and understanding a wide range of phenomena in natural science, for example fluid dynamics, quantum mechanics and aerodynamics. PDEs provides granular representation of physical processes. Traditionally, numerical simulations of PDEs are applied to analyze complex physical process that provides analytical solutions. However, achieving precise simulations for PDEs usually requires substantial time and computational cost since a fine-grained optimized search is required in spatial or temporal domains.

Machine Learning modeling offer solutions to the challenges. Fourier Neural Operator (FNO) [1] offers significant efficiency and resolution invariant attributes. FNO leverages neural networks with Fourier transforms to map its input function to the target function in the frequency domain, which offers notable superior performance compared to traditional Convolutional Neural Networks (CNNs). There are considerable research leveraging FNO, including but not limited to forecasting, stress-strain analysis [2], and solving seismic wave equations [3].

In this study, we aim to address the challenges of modeling tumor growth using partial differential equations (PDEs) of the reaction-diffusion type, which capture the spatial dynamics of tumor cell density and its proliferative and invasive behaviors. Traditional approaches, such as finite element methods (FEM) and finite difference methods (FDM), require finely discretized spatial meshes, leading to high computational costs and inefficiencies. Neural operators offer a promising alternative by being mesh-independent [4], enabling training on one mesh and evaluation on another, thus allowing for greater flexibility. Unlike standard deep learning models like Convolutional Neural Networks (CNNs), neural operators are parameterized in function space, learning continuous functions rather than discretized representations [5]. Specifically, the Fourier Neural Operator (FNO) stands out by applying Fourier transforms to map input functions to target functions in the frequency domain, offering superior performance over CNNs through its use of global Fourier filters. This project will utilize FNO to predict the progression of tumor growth by applying it to initial tumor density maps.

II. METHODOLOGY

A. FUNDAMENTALS

Reaction-diffusion equations describe the evolution of a scalar field $u(x,t)$ representing the tumor cell density over space $x \in \Omega \subset R^d$ and time $t \geq 0$. The PDE is given by:

$$\frac{\partial u}{\partial t} = D\nabla^2 u + f(u), \tag{1}$$

where D is the diffusion coefficient representing the spread of tumor cells, ∇^2 denotes the Laplace operator capturing spatial diffusion, and $f(u)$ represents the reaction term, which models the proliferation of tumor cells. Traditional methods like finite difference methods (FDM) or finite element methods (FEM) discretize the spatial domain Ω into a fine grid to solve the PDE, but this becomes computationally expensive as the resolution of the mesh increases.

The Fourier Neural Operator (FNO) offers a novel approach to solving PDEs like this by learning mappings between function spaces rather than discretized vectors. Specifically, given an input function $a(x)$, which might represent initial conditions such as the initial tumor density $u(x,0)$, the FNO aims to learn an operator G such that:

$$G(a) \approx u(x,T), \tag{2}$$

where $u(x,T)$ is the solution of the PDE at time T. Unlike traditional deep learning models, which operate on

discretized input data, the FNO parameterizes G directly in the function space, allowing for greater flexibility and mesh independence.

The core idea behind the FNO is to transform the input function into the frequency domain using the Fourier transform. Let $\hat{a}(k)$ denote the Fourier transform of the input $a(x)$:

$$\hat{a}(k) = \mathcal{F}(a)(k) = \int_{\Omega} a(x) e^{-2\pi i k \cdot x} \, dx, \tag{3}$$

where k represents the frequency components. The FNO learns a mapping in this transformed space using a series of neural network layers to parameterize the integral kernel in the Fourier domain. The transformation is then inverted back to the spatial domain using the inverse Fourier transform:

$$\tilde{u}(x) = \mathcal{F}^{-1}(K(k) \cdot \hat{a}(k))(x), \tag{4}$$

where $K(k)$ represents the learned integral kernel in the Fourier space. The parameterization of the kernel in the frequency domain allows the FNO to capture the global interactions across the entire domain Ω, unlike CNNs which rely on local convolutions.

The architecture of the FNO can be summarized as follows: given an input function a, it is first lifted to a higher-dimensional representation using a pointwise neural network P. The resulting representation is then transformed into the frequency domain, and a sequence of Fourier layers is applied. Each Fourier layer operates as:

$$v_{j+1} = \sigma\left(\mathcal{F}^{-1}\left(\kappa_j \cdot \mathcal{F}(v_j)\right) + W_j v_j\right), \tag{5}$$

where v_j represents the state at the j-th layer, κ_j is the Fourier representation of the kernel at that layer, W_j is the learned linear transformation, and σ is a non-linear activation function.

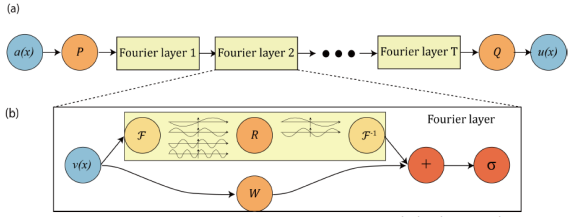

Fig. 1: The architecture of (a) Neural Operator and (b) Fourier Layer.

The final output v_L is then projected back to the original function space using a pointwise neural network Q, yielding the solution approximation:

$$G(a) \approx Q(v_L). \tag{6}$$

By learning in the frequency domain, the FNO can efficiently capture both local and global interactions in the input function, making it well-suited for solving reaction-diffusion PDEs over large spatial domains. In the context of tumor growth modeling, this approach allows for accurate predictions of the spatial distribution of tumor cells across different resolutions of the initial density map, providing a powerful tool for simulating tumor progression dynamics.

B. Brain Tumor Modeling Simulated Data

The simulation of tumor growth dynamics relies on a reaction-diffusion model that captures the interplay between tumor cell proliferation and spatial spread. The reaction-diffusion equation used is:

$$\frac{\partial n}{\partial t} = D\nabla^2 n + rn\left(1 - \frac{n}{n_{\text{max}}}\right), \tag{7}$$

where n represents the tumor cell density, D is the diffusion coefficient, r is the reaction rate, and n_{max} is the maximum carrying capacity of the tumor cells. The diffusion term ($D\nabla^2 n$) models the spatial spread of cells, while the reaction term ($rn(1 - n/n_{\text{max}})$) represents the proliferation and saturation dynamics of tumor growth.

The diffusion coefficient (D) is sampled uniformly from the range $[0.0001, 0.01]$ mm^2/day, reflecting the variability in tumor cell motility across different biological scenarios. The reaction rate (r) is sampled from $[0.01, 0.1]$ 1/day, capturing the variability in tumor growth aggressiveness. These ranges were chosen to encompass realistic biological conditions observed in clinical and experimental studies [6]–[12].

The spatial domain is a cube with dimensions $L = 31.0$ mm, discretized into a $31 \times 31 \times 31$ grid, resulting in a grid spacing of $\Delta x = \Delta y = \Delta z = L/(N-1) \approx 1.0$ mm. The temporal domain spans $T = 50.0$ days, divided into 1500 time steps, yielding a temporal resolution of $\Delta t = T/N_t \approx 0.033$ days. This fine spatial and temporal resolution ensures numerical stability and accuracy in capturing tumor evolution over the specified domain.

The initial tumor cell density is modeled as a Gaussian distribution centered at the middle of the domain, given by:

$$n_0(x, y, z) = A \exp\left(-\frac{(x - L/2)^2}{2\sigma^2} - \frac{(y - L/2)^2}{2\sigma^2} - \frac{(z - L/2)^2}{2\sigma^2}\right), \tag{8}$$

where $A = 1.0$ is the peak cell density, and $\sigma = 2.0$ mm controls the spread of the initial distribution. This setup mimics a localized tumor at the onset of growth.

The simulation iteratively updates the tumor cell density at each time step using a finite difference approximation of the reaction-diffusion equation. The Laplacian operator is implemented with a convolution kernel, and the time integration uses an explicit forward Euler scheme. The results are saved for each simulation, allowing for a comprehensive analysis of how variations in D and r influence tumor growth dynamics over time and space.

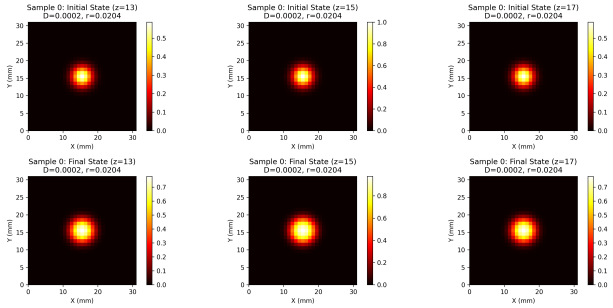

Fig. 2: Tumor evolution for $D = 0.0002$ and $r = 0.02$. Top row: Initial state. Bottom row: Final state. Each column corresponds to a different z-slice of the 3D domain.

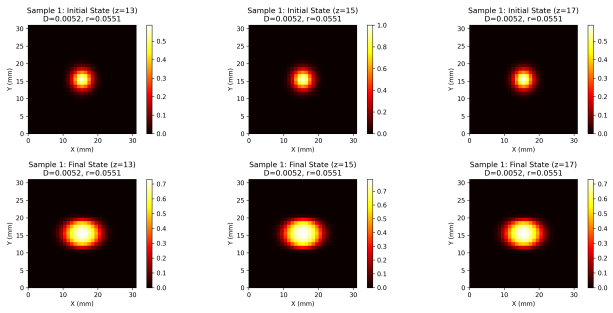

Fig. 3: Tumor evolution for $D = 0.005$ and $r = 0.05$. Top row: Initial state. Bottom row: Final state. Each column corresponds to a different z-slice of the 3D domain.

C. Model Architecture and Training

The model architecture consists of two main components: a Fourier Neural Operator (FNO3D) and a convolutional neural network (TumorGrowthCNN), each designed to process 3D volumetric data for modeling tumor growth dynamics.

1) FNO3D Architecture: The `FNO3D` model is built to solve reaction-diffusion equations in 3D space by leveraging Fourier transforms for efficient computation in the frequency domain. It includes three convolutional layers:

- **Initial Fourier Layer:** A 3D convolutional layer with a kernel size of 1 transforms the input into a higher-dimensional representation with a specified width or modes (32 channels).
- **Intermediate Fourier Layers:** Additional convolutional layers are applied to the real and imaginary parts of the Fourier-transformed input to learn representations in the frequency domain.
- **Final Fourier Layer:** A 3D convolution reduces the processed data back to a single output channel.

The forward pass includes a Fourier transform (`torch.fft.fftn`) to map spatial data into the frequency domain, convolutional operations on the real and imaginary components, and an inverse Fourier transform (`torch.fft.ifftn`) to return to the spatial domain. The final convolution layer refines the output to match the desired scalar field representation.

2) TumorGrowthCNN Architecture: The `TumorGrowthCNN` is a standard convolutional neural network (CNN) designed to predict tumor growth dynamics.

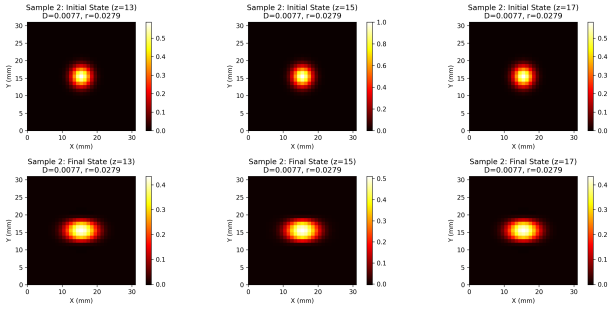

Fig. 4: Tumor evolution for $D = 0.007$ and $r = 0.02$. Top row: Initial state. Bottom row: Final state. Each column corresponds to a different z-slice of the 3D domain.

It consists of:

- **Convolutional Layers:** Four 3D convolutional layers with increasing channel depths (16, 32, 64, and 1) extract spatial features.
- **Batch Normalization:** Applied after the first three convolutional layers to stabilize and accelerate training.
- **ReLU Activation:** Introduced after each batch normalization to introduce non-linearity.
- **Output Layer:** A final 3D convolutional layer reduces the output to a single channel, representing the scalar prediction.

3) Training and Optimization: The `FNO3D` model is trained with the `Adam` optimizer and a learning rate of 1×10^{-4} for 500 epochs. The training loop processes 3D data, adding a channel dimension to match the expected input size. The model minimizes different loss function (mean square error, mean absolute error, huber loss, combined loss) to predict the final tumor state from initial conditions. The loss is computed over batches, and gradients are backpropagated to update the model's weights.

During each epoch, both training and validation losses are calculated to monitor model performance and ensure generalization. By combining the strengths of FNO3D and CNN architectures, the model effectively captures both local and global spatial dependencies in tumor growth simulations.

III. Results

We evaluate the performance of the Fourier Neural Operator (FNO) and Convolutional Neural Network (CNN) architectures using several performance metrics: Root Mean Squared Error (RMSE), Mean Absolute Error (MAE), R^2 score, Peak Signal-to-Noise Ratio (PSNR), Structural Similarity Index (SSIM), Dice Similarity Coefficient (DSC), and Mean Absolute Percentage Error (MAPE). The performance metrics used to evaluate the models include RMSE (Root Mean Squared Error), which measures the average magnitude of the errors between predicted and actual values; MAE (Mean Absolute Error), which quantifies the average absolute difference between predictions and actual values; and R^2 (R-squared), which indicates the proportion of variance in the data explained by the model. PSNR (Peak Signal-to-Noise Ratio) assesses the quality of image reconstruction, while SSIM (Structural Similarity Index) measures the similarity

between two images. The Dice Similarity Coefficient quantifies the overlap between predicted and actual tumor regions, and MAPE (Mean Absolute Percentage Error) evaluates the percentage error in predictions.

A. Performance Metrics for FNO and CNN Models

The CNN model outperforms the FNO model across most performance metrics, including RMSE, MAE, R^2 score, PSNR, SSIM, and Dice Similarity Coefficient as presented in Table I. Specifically, the CNN demonstrates lower RMSE and MAE, indicating more accurate predictions, and achieves a higher R^2 score, reflecting a stronger correlation between the predicted and actual tumor growth values. The CNN also excels in PSNR, suggesting better image reconstruction quality, and has a higher Dice Similarity Coefficient, indicating better overlapping between predicted and ground truth. Both models show very high MAPE values, likely due to extreme predictions or outliers, but the CNN's superior performance across multiple metrics makes it the more reliable model for tumor growth prediction in this study.

TABLE I: Performance metrics for the FNO and CNN models on tumor growth prediction.

Metric	FNO Results	CNN Results
RMSE	0.0565	0.0362
MAE	0.0195	0.0077
R^2 Score	0.5178	0.7911
PSNR (dB)	25.17	29.04
SSIM	0.9991	0.9995
Dice Similarity Coefficient	0.3812	0.5962
MAPE (%)	3.504×10^{24}	3.188×10^{23}

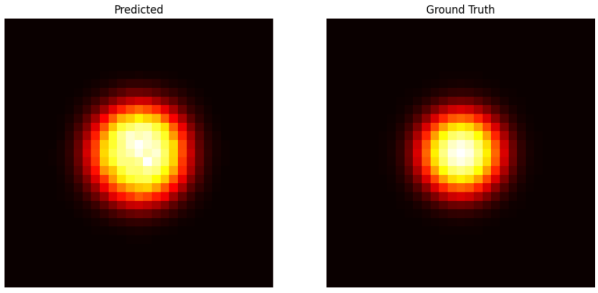

Fig. 5: CNN Predicted and Ground Truth Results (MSE Loss)

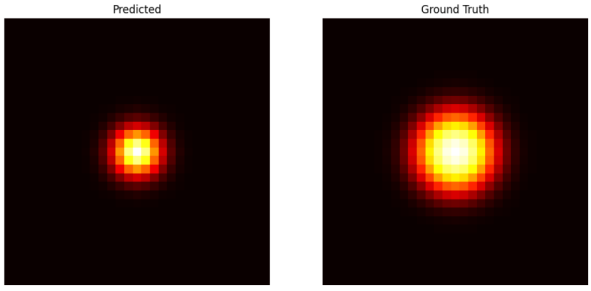

Fig. 6: FNO Predicted and Ground Truth Results (MSE Loss)

B. Ablation Study

The choice of loss function plays a crucial role in model training, as it determines how well the model learns and generalizes. In this study, we used three different loss functions: Mean Absolute Error (MAE), Huber loss, and a combined loss (SSIM and Huber loss). The MAE loss focuses on minimizing the average absolute difference between the predicted and actual values, while the Huber loss combines the advantages of both MAE and Mean Squared Error (MSE), making it more robust to outliers. The combined loss function incorporates SSIM to better capture structural similarity between predicted and ground truth images, alongside Huber loss to ensure smooth training. We present the performance metrics for the FNO and CNN models trained with these loss functions in the following Table II.

TABLE II: Performance Metrics for FNO and CNN Models Trained with Different Loss Functions

Metric	MAE Loss	Huber Loss	Combined Loss
Model *FNO*			
RMSE	0.0566	0.0564	0.0617
MAE	0.0138	0.0168	0.0110
R^2 Score	0.5178	0.5195	0.4124
PSNR	25.18	25.19	24.31
SSIM	0.9990	0.9991	0.9991
Dice Similarity	0.3812	0.3812	0.5272
MAPE	$1.48 \times 10^{24}\%$	$2.43 \times 10^{24}\%$	$2.22 \times 10^{23}\%$
Model *CNN*			
RMSE	0.0379	0.0364	0.0384
MAE	0.0075	0.0076	0.0077
R^2 Score	0.780	0.7861	0.7749
PSNR	29.04	29.00	28.63
SSIM	0.9995	0.9995	0.9995
Dice Similarity	0.5962	0.6169	0.5424
MAPE	$3.19 \times 10^{23}\%$	$2.02 \times 10^{23}\%$	$1.92 \times 10^{23}\%$

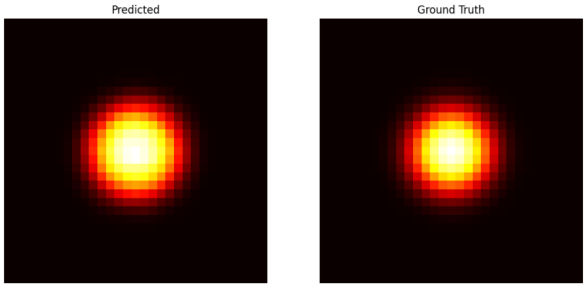

Fig. 7: CNN Predicted and Ground Truth Results (MAE Loss)

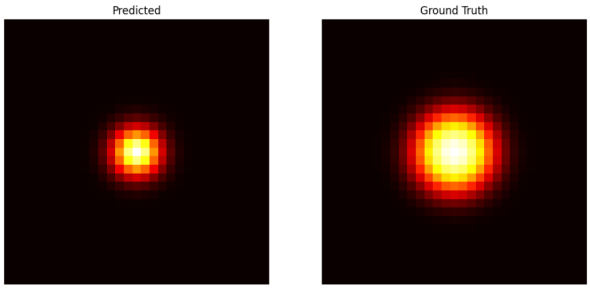

Fig. 8: FNO Predicted and Ground Truth Results (MAE Loss)

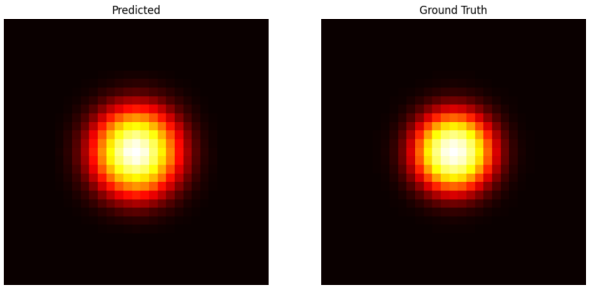

Fig. 9: CNN Predicted and Ground Truth Results (Huber Loss)

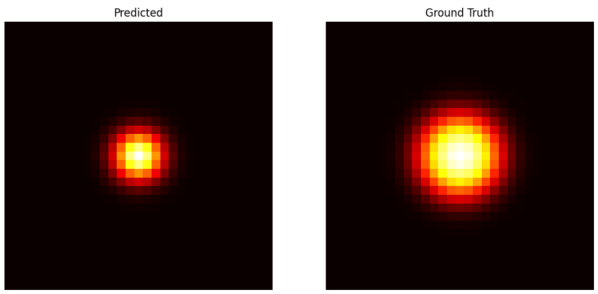

Fig. 10: FNO Predicted and Ground Truth Results (Huber Loss)

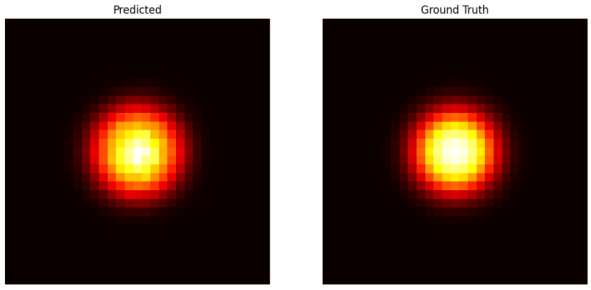

Fig. 11: CNN Predicted and Ground Truth Results (Combined Loss)

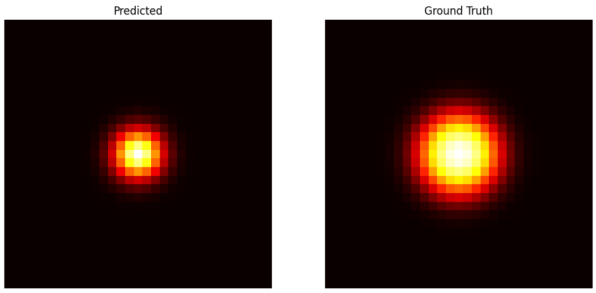

Fig. 12: FNO Predicted and Ground Truth Results (Combined Loss)

C. Mode Comparison in FNO

In the FNO model, different modes (8, 16, 32, 128, 256) represent different configurations of the model's network, primarily indicating the number of modes (Fourier basis functions) used for the spectral representation of the input data. The choice of modes can significantly affect the model's performance. Generally, as the number of modes increases, the model may capture more complex features, potentially leading to better generalization and performance. However, the performance gain can diminish beyond a certain point, and the model may become computationally expensive with higher modes. The results for each mode configuration presented in Table III.

The performance of the FNO model varies slightly across different mode configurations. For lower modes (Mode-8, Mode-16), the model tends to show a slight increase in RMSE and MAE, indicating a possible reduction in model accuracy. The R^2 score, which reflects the variance explained by the model, is slightly higher for Mode-128 and Mode-256, suggesting that the model starts capturing more of the data's complexity as the number of modes increases. However, the differences in metrics like PSNR, SSIM, and Dice Similarity are minimal across modes, implying that the higher modes do not significantly improve image quality or structural similarity in this specific case. The MAPE also follows a decreasing trend with higher modes, indicating a reduction in percentage error. Overall, Mode-256 yields the best overall performance with the highest R^2 score and PSNR. However, the performance gain is marginal compared to Mode-128, suggesting that a configuration of Mode-128 may offer a good trade-off between model complexity and performance.

IV. CONCLUSIONS

In this study, we explored the performance of different architectures and loss functions for tumor growth prediction using the Fourier Neural Operator (FNO) and Convolutional Neural Network (CNN) models. We evaluated the models across several metrics including RMSE, MAE, R^2 score, PSNR, SSIM, Dice Similarity Coefficient, and MAPE to provide a comprehensive understanding of their predictive accuracy and robustness.

The results showed that the CNN model consistently outperformed the FNO model in terms of RMSE, MAE, R^2 score, and PSNR, particularly when using Mean Squared Error (MSE) as the loss function. Notably, CNN also performed better with other loss functions such as MAE, Huber loss, and combined loss (SSIM and Huber), showing promising improvements in the ability to predict tumor regrowth.

Further, the evaluation of different modes in the FNO model (with mode sizes of 8, 16, 32, 128, and 256) demonstrated that larger modes generally resulted in a slight improvement in the model's performance, particularly in terms of the R^2 score and PSNR, while maintaining high SSIM values. Despite these improvements, the performance was still lower compared to CNN in terms of predictive accuracy.The FNO could not perform as well as the CNN in this study likely due to its inherent design and the way it handles spatial dependencies in the data. FNO relies on the Fourier transform to approximate solutions to partial differential equations, which works well for continuous and structured data. However, it may not capture complex, localized features in medical imaging data as effectively as CNNs. CNNs are specifically designed to learn hierarchical features through convolutional layers, making them highly adept at detecting spatial patterns and structures, which is crucial for

TABLE III: Performance Metrics for FNO with Different Mode Configurations

Metric	Mode-8	Mode-16	Mode-32	Mode-128	Mode-256
RMSE	0.0632	0.0640	0.0628	0.0625	0.0622
MAE	0.0108	0.0108	0.0106	0.0109	0.0106
R^2 Score	0.3791	0.3610	0.387	0.3942	0.4019
PSNR	24.08	23.96	24.129	24.18	24.23
SSIM	0.9991	0.9991	0.999	0.9991	0.9991
Dice Similarity	0.5272	0.5272	0.527	0.5272	0.5272
MAPE	$1.12 \times 10^{23}\%$	$9.70 \times 10^{22}\%$	$7.22 \times 10^{22}\%$	$2.12 \times 10^{23}\%$	$7.11 \times 10^{22}\%$

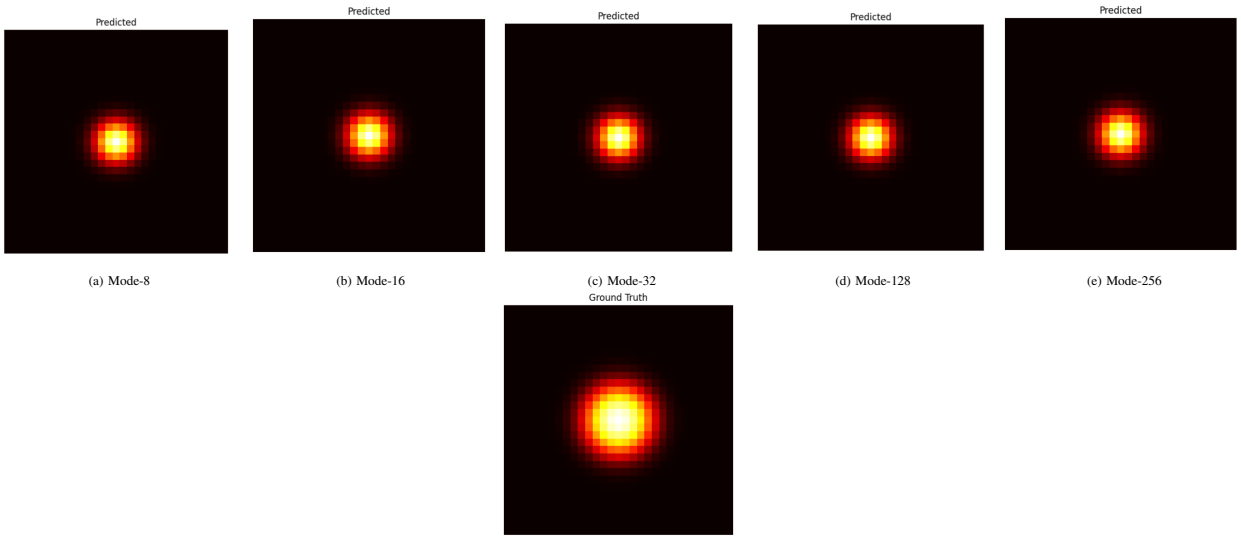

(a) Mode-8 (b) Mode-16 (c) Mode-32 (d) Mode-128 (e) Mode-256

(f) Ground Truth (GT)

Fig. 13: Comparison of GT and different modes (8, 16, 32, 128, 256) results in FNO

tasks like tumor prediction. Additionally, CNNs typically perform better with image-specific loss functions, like MAE, SSIM, or combined loss functions, which are optimized for pixel-wise comparisons. On the other hand, FNO's global approach may overlook finer-grained local details, making it less suited for the pixel-level precision required in medical imaging tasks, leading to its lower performance compared to CNN.

The findings highlight the significant potential of CNN-based models for medical image analysis, while also indicating that FNO, with the appropriate configurations, can still be a viable alternative. This study also underscores the importance of selecting the right model architecture and loss function to optimize performance in medical imaging tasks.

Future work will focus on further tuning these models, exploring hybrid architectures, and expanding the evaluation to include a larger dataset to confirm these results across different imaging modalities.

REFERENCES

[1] Z. Li, D. Z. Huang, B. Liu, and A. Anandkumar, "Fourier Neural Operator with Learned Deformations for PDEs on General Geometries," *International Conference on Learning Representations (ICLR)*,vol. 24, pp. 1–26, 2022, doi: 10.5555/3648699.3649087.

[2] Y. Yang, A. F. Gao, J. C. Castellanos, Z. E. Ross, K. Azizzadenesheli, and R. W. Clayton, "Seismic Wave Propagation and Inversion with Neural Operators," *Seism. Rec.*, vol. 1, no. 3, pp. 126–134, 2021, doi: 10.1785/0320210026.

[3] N. Kovachki et al., "Neural Operator: Learning Maps Between Function Spaces With Applications to PDEs," *J. Mach. Learn. Res.*, vol. 24, pp. 1–97, 2023.

[4] K. C. L. Wong, H. Wang, and T. Syeda-Mahmood, "FNOSeg3D: Resolution-Robust 3D Image Segmentation with Fourier Neural Operator," *Proc. - Int. Symp. Biomed. Imaging*, vol. 2023-April, pp. 1–5, 2023, doi: 10.1109/ISBI53787.2023.10230586.

[5] A. Gurrala, K. Arora, H. Sharma, S. Qamar, A. Roy, and S. Chakraborty, "Classification of High-Resolution Chest CT Scan Images Using Adaptive Fourier Neural Operators for COVID-19 Diagnosis," *Covid*, vol. 4, no. 8, pp. 1236–1244, 2024, doi: 10.3390/covid4080088.

[6] C. Meaney, S. Das, E. Colak, and M. Kohandel, "Deep learning characterization of brain tumours with diffusion weighted imaging," *J. Theor. Biol.*, vol. 557, pp. 1–16, 2023, doi: 10.1016/j.jtbi.2022.111342.

[7] P. K. Burgess, P. M. Kulesa, J. D. Murray, and E. C. J. Alvord, "The interaction of growth rates and diffusion coefficients in a three-dimensional mathematical model of gliomas.," *J. Neuropathol. Exp. Neurol.*, vol. 56, no. 6, pp. 704–713, Jun. 1997.

[8] H. Akbari et al., "Imaging surrogates of infiltration obtained via multiparametric imaging pattern analysis predict subsequent location of recurrence of glioblastoma," *Neurosurgery*, vol. 78, no. 4, pp. 572–580, 2016, doi: 10.1227/NEU.0000000000001202.

[9] B. H. Menze, E. Stretton, E. Konukoglu, and N. Ayache, "Image-based modeling of tumor growth in patients with glioma," *Optim. Control Image Process.* Springer, Heidelb., pp. 1–12, 2011.

[10] P. Tracqui, G. C. Cruywagen, D. E. Woodward, G. T. Bartoo, J. D. Murray, and E. C. J. Alvord, "A mathematical model of glioma growth: the effect of chemotherapy on spatio-temporal growth.," *Cell Prolif.*, vol. 28, no. 1, pp. 17–31, Jan. 1995, doi: 10.1111/j.1365-2184.1995.tb00036.x.

[11] D. E. Woodward, J. Cook, P. Tracqui, G. C. Cruywagen, J. D. Murray, and E. C. Alvord, "A mathematical model of glioma growth: The effect of extent of surgical resection," *Cell Prolif.*, vol. 29, no. 6, pp. 269–288, 1996, doi: 10.1111/j.1365-2184.1996.tb01580.x.

[12] C. H. Wang et al., "Prognostic significance of growth kinetics in newly diagnosed glioblastomas revealed by combining serial imaging with a novel biomathematical model," *Cancer Res.*, vol. 69, no. 23, pp. 9133–9140, 2009, doi: 10.1158/0008-5472.CAN-08-3863. .